Renewable Energy 107 (2017) 373–385

Contents lists available at ScienceDirect

Renewable Energy

journal homepage: www.elsevier.com/locate/renene

CFD simulation of a vertical axis wind turbine operating at a moderate tip speed ratio: Guidelines for minimum domain size and azimuthal increment

Abdolrahim Rezaeiha [a, *], Ivo Kalkman [a], Bert Blocken [a, b]

[a] Building Physics and Services, Department of the Built Environment, Eindhoven University of Technology, P.O. Box 513, 5600 MB, Eindhoven, The Netherlands

[b] Building Physics Section, Department of Civil Engineering, KU Leuven, Kasteelpark Arenberg 40 – Bus 2447, 3001, Leuven, Belgium

ARTICLE INFO

Article history:
Received 9 August 2016
Received in revised form
9 January 2017
Accepted 4 February 2017
Available online 5 February 2017

Keywords:
Vertical axis wind turbine (VAWT)
CFD
Guideline
Domain size
Azimuthal increment
Number of revolutions

ABSTRACT

Accurate prediction of the performance of a vertical-axis wind turbine (VAWT) using Computational Fluid Dynamics (CFD) simulation requires a domain size that is large enough to minimize the effects of blockage and uncertainties in the boundary conditions on the results. It also requires the employment of a sufficiently fine azimuthal increment ($d\theta$) combined with a grid size at which essential flow characteristics can be accurately resolved. The current study systematically investigates the effect of the domain size and azimuthal increment on the performance of a 2-bladed VAWT operating at a moderate tip speed ratio of 4.5 using 2-dimensional and 2.5-dimensional simulations with the unsteady Reynolds-averaged Navier-Stokes (URANS). The grid dependence of the results is studied using three systematically refined grids. The turbine has a low solidity of 0.12 and a swept area of 1 m^2. Refining $d\theta$ from 10.0° to 0.5° results in a significant (≈43%) increase in the predicted power coefficient (C_P) while the effect is negligible (≈0.25%) with further refinement from 0.5° to 0.05° at the given λ. Furthermore, a distance from the turbine center to the domain inlet and outlet of 10D (D: diameter of turbine) each, a domain width of 20D and a diameter of the rotating core of 1.5D are found to be safe choices to minimize the effects of blockage and uncertainty in the boundary conditions on the results.

1. Introduction

Recently, vertical-axis wind turbines (VAWTs) have received growing interest for wind energy harvesting offshore [1] as well as in the urban environment [2–5]. For offshore application this can be attributed to their scalability, reliability and low installation and maintenance costs, while for environments with frequent changes in wind direction such as urban environments their omni-directional capability is their main advantage. However, due to a comparatively small amount of research on VAWTs in the last 2-3 decades, their performance is currently lower than that of their horizontal-axis counterparts. The current renewed interest has resulted in more research and further understanding of VAWT flow complexities. These complexities include dynamic stall [6,7], flow curvature effects [8], blade-wake interactions and unsteady 3D wake dynamics [9]. Increased understanding of the aerodynamics of VAWTs has enabled further optimization of their performance which has been conducted using low-to moderate-fidelity inviscid modeling [10,11], high-fidelity viscous CFD simulations [12,13] and wind tunnel tests [9].

Accurate prediction of VAWT performance using CFD simulation requires a sufficiently fine azimuthal increment ($d\theta$) and grid resolution in order to resolve essential flow details both in time and space. The domain size with respect to the turbine diameter (D) also needs to be sufficiently large in order to minimize the influence of blockage (which is a result of the presence of the turbine in the domain and the boundary conditions at the lateral boundaries) as well as the uncertainties regarding flow conditions at the other boundaries of the domain. Minimum requirements for the domain size have been studied for several types of flow, e.g. urban flows [14–16] and best practice guidelines have been published in order to minimize unwanted effects of the boundaries. However, although numerous CFD studies of VAWTs have recently been published there is no consistency in the employed domain size and azimuthal increment, and very few of them have systematically

* Corresponding author.
E-mail address: a.rezaeiha@tue.nl (A. Rezaeiha).

http://dx.doi.org/10.1016/j.renene.2017.02.006

Nomenclature

A	swept area, H.D [m^2]
BR	blockage ratio (D/W) [−]
c	blade chord length [m]
C_m	instantaneous moment coefficient [−]
C_P	power coefficient [−]
C_T	thrust coefficient [−]
CoP	pressure coefficient [−]
D	turbine diameter [m]
d_c	diameter of rotating core [m]
d_i	distance to the domain inlet from turbine center [m]
d_o	distance to the domain outlet from turbine center [m]
d_{up}	upstream distance to the turbine center [m]
dt	time step [s]
dθ	azimuthal increment [°]
F_s	safety factor [−]
H	turbine height [m]
L	domain length [m]
M	moment [Nm]
q	dynamic pressure [Pa]
R	turbine radius [m]
Re	chord-based Reynolds number [−]
Re_θ	momentum thickness Reynolds number [−]
Re_{geo}	Reynolds number from geometrical relations [−]
T	thrust force [N]
u	time-averaged streamwise velocity [m/s]
U	velocity magnitude [m/s]
U_∞	freestream velocity [m/s]
v	time-averaged lateral velocity [m/s]
W	domain width [m]
W_{geo}	resultant velocity from geometrical relations [m/s]
α_{geo}	geometrical angle of attack [°]
γ	intermittency [−]
λ	tip speed ratio, $\Omega.R/U_\infty$ [−]
ν	kinematic viscosity [m^2/s]
θ	azimuthal angle [°]
ρ	density [kg/m^3]
σ	solidity, n.c/D [−]
ω	specific dissipation rate [1/s]
Ω	rotational speed [rad/s]

investigated the sensitivity of the results to these computational parameters [17]. The few studies which do exist on azimuthal increment (for HAWTs [18] and VAWTs [12,19–22]) and domain size (for HAWTs [23,24] and for VAWTs [12,25–27]), although very valuable, are too limited in scope to derive reliable minimum requirements. Deriving such best practice guidelines is therefore the topic of the present study.

The current study first investigates the number of revolutions of the turbine which is needed to obtain a converged solution for a VAWT operating at a moderate tip speed ratio (λ) of 4.5 and sets this as a convergence criterion for all subsequent simulations. A sensitivity analysis is then performed for the computational grid size, dθ and domain size in order to find minimum values where the VAWT performance (power and thrust coefficients, C_P and C_T) can be considered independent of these parameters. These values can then be used as guidelines to ensure the accuracy of CFD results in case the turbine is operating at a moderate λ and the flow on the blades is not strongly separated. It is important to note that the focus of the current study is merely on an urban-scale VAWT with low solidity operating at a moderate tip speed ratio. The selected geometrical and operational characteristics of the turbine simplify the flow physics and facilitate the identification of guidelines as explained below.

- The low solidity reduces the complexities associated to blade-wake interactions and flow curvature effects [8,9].
- The moderate tip speed ratio corresponds to the regime where a VAWT operates most optimally because the variations of angle of attack are closer to the design angle of attack of the employed airfoil and large separation is therefore avoided [7,9]. In the current study, a symmetric airfoil with zero pitch angle is employed. Using an asymmetric airfoil or a different pitch angle might result in large separation on blades even at a moderate tip speed ratio. Therefore, for each simulation the variations of angle of attack during the revolution should be taken into account. Low tip speed ratios can also result in large separation for a turbine with similar geometrical characteristics (solidity, airfoil shape and pitch angle) [13]. Furthermore, as a result of the aforementioned geometrical and operational characteristics of the turbine, dynamic stall on the blades is avoided [9], which further limits complexities of the flow and dynamic loads on the blades.
- The scale of the VAWT investigated corresponds to a chord-based Reynolds number $Re > 10^5$. Due to strong Reynolds number effects for flow over airfoils [28–30], for very small turbines where the range of Re is different ($Re < 10^5$), separation can happen earlier and blades might experience large separation under the same operating conditions.

The paper starts with a description of the methodology in section 2 which includes the geometrical and operational characteristics of the turbine, the computational domain and grid, the numerical settings and the test matrices describing the details of the parametric studies. Then, the sensitivity of the results to the number of revolutions of the turbine before data sampling (section 3.1) and grid resolution (section 3.2) are analyzed. The validation with experimental data [9] is subsequently performed (section 4). Finally the results of the sensitivity study on the domain size and dθ are discussed in sections 5 and 6, respectively. Discussion and conclusions are presented in section 7–8.

2. Methodology

2.1. VAWT geometrical and operational characteristics

A 2-bladed H-type low-solidity VAWT equipped with symmetric NACA0018 airfoils, a diameter (D) and height (H) of both equal to 1 m, a swept area (A) of 1 m^2 and a solidity (σ) of 0.12 is simulated in 2D and 2.5D at a constant λ of 4.5. The 2D simulation represents the midplane of a turbine with high aspect ratio; where the 3D tip effects are small; and is selected after the comparison with results from a 2.5D simulation showed a negligible (<0.25%) difference in power and thrust coefficients (C_P and C_T) for the given tip speed ratio and solidity (described in section 4). The low-solidity of the turbine is selected to limit the blade-wake interactions. The λ value is selected to ensure that the angle of attack of the blades remains below the static stall angle for the airfoil in order to avoid dynamic stall. In order to check that this is indeed the case the blade Reynolds number for the given λ is calculated based on geometrical relations for VAWTs using Eqns. (1) and (2) [31] and found to be in

the range 100,000 < Re_{geo} < 200,000; in this range the static stall angle of the airfoil is approximately 14° [32] while the maximum geometrical angle of attack (calculated using Eqn. (3) [31]) is less than 13°. The experienced angle of attack will be even lower than the geometrical value as α_{geo} is defined from geometrical relations based on the assumption of zero induced velocity while a non-zero value results in a lower experienced streamwise velocity, and therefore a lower experienced angle of attack. This limits the 3D effects in the flow in the midplane of the VAWT. Furthermore, this is the range where the VAWTs operate optimally and is therefore of greatest interest for practical applications. The turbine has a shaft with a 0.04 m diameter which is rotating in the same direction as the turbine. The turbine rotational velocity (Ω) is 83.8 rad/s (800 rpm) and the free-stream velocity is 9.3 m/s. The geometrical and operational characteristics of the VAWT are presented in Table 1.

$$W_{geo} = U_\infty \sqrt{\lambda^2 + 2\lambda \cos\theta + 1} \quad (1)$$

$$\mathrm{Re}_{geo} = \frac{W_{geo} c}{\nu} \quad (2)$$

$$\alpha_{geo} = \tan^{-1}\left[\frac{\sin\theta}{\cos\theta + \lambda}\right] \quad (3)$$

2.2. Computational domain and grid

The computational domain shown in Fig. 1 consists of a rotating core where the turbine is located and a fixed domain surrounding the core. A non-conformal interface with sliding grid between the fixed domain and the rotating core enables rotation of the turbine. The blade orbit is divided into four quartiles [33]: upwind (45° ≤ θ < 135°), leeward (135° ≤ θ < 225°), downwind (225° ≤ θ < 315°) and windward (315° ≤ θ < 45°).

Through systematic variation of d_i, d_o, W and d_c (see Fig. 1) the effect of these parameters on C_P and C_T of the turbine are investigated: Table 2 describes the details of the studied cases. The effect of dθ is also studied for various cases, as detailed in Table 3; a value of 0.1° is used for the reference case. The 2.5D domain is based on the reference case with a span of 0.06 m, equal to the chord of the airfoil.

For all the cases a computational grid is generated which consists of quadrilateral cells. The boundary layer grid is employed on the walls (airfoils and shaft). The cell size is equal at both sides of the interface between the rotating and fixed domains in order to minimize numerical errors at this interface. The maximum y^+ is below 4 on the airfoils and below 2 on the shaft in order to accurately capture the linear viscous sublayer. Images of the reference computational grid for the 30D × 20D (L × W) domain size highlighting different parts of the grid are shown in Fig. 2. The independence of the results to the computational grid is studied using 2 finer grids (see Table 4), which also serves to quantify the discretization error. The computational grid for the 2.5D domain is based on the coarse grid ground plane which is extruded in the third dimension in a non-conformal manner with cell sizes of 0.5×10^{-3} m, 1.0×10^{-3} m and 2.0×10^{-3} m on the airfoils, shaft and fixed domain, respectively (see Fig. 2).

Table 1
Geometrical and operational characteristics of the VAWT.

Characteristics	Turbine
Number of blades, n	2
Diameter, D [m]	1
Height, H [m]	1
Swept area, A [m^2]	1
Solidity, σ [−]	0.12
Airfoil	NACA0018
Airfoil chord, c [m]	0.06
Shaft diameter [m]	0.04
Tip speed ratio, λ [−]	4.5
Freestream velocity, U_∞ [m/s]	9.3
Rotational speed, Ω [rad/s]	83.8

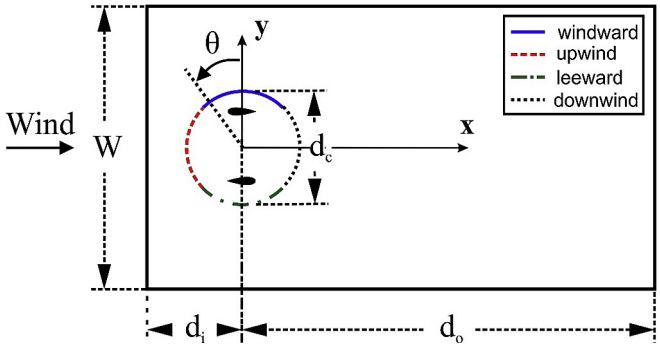

Fig. 1. Schematic of the computational domain: d_i, distance from the inlet to the turbine center; d_o distance from the turbine center to the outlet; d_c, diameter of the core region; W, width of the computational domain.

2.3. Numerical settings

The incompressible unsteady Reynolds-averaged Navier-Stokes (URANS) equations are solved using the commercial CFD software package ANSYS Fluent 16.1 [34]. The SIMPLE scheme is used for pressure-velocity coupling and 2nd order discretization is employed both in time and space. The boundary conditions at the inlet, outlet, side faces and walls are uniform velocity, zero surface-averaged gauge pressure, symmetry and no slip, respectively. A freestream velocity (U_∞) of 9.3 m/s with a turbulence intensity of 5% is set at the inlet while the incident flow turbulence intensity is 4.42% due to the decay in the domain. The incident value is defined as the value that would occur at the location of the turbine, if the turbine would be absent [35,36].

Turbulence is modeled using the 4-equation transition SST turbulence model [37]. The performance of the turbine is strongly dependent on the development of the boundary layer on the blades and therefore an accurate prediction of the transition onset is essential. In addition to the equations for turbulent kinetic energy k and specific dissipation rate ω employed in the k-ω SST model, the 4-equation transition SST model [37] solves two more equations for the intermittency (γ) and momentum thickness Reynolds number (Re_θ) which should lead to a better prediction of the laminar to turbulent transition onset [38].

Calculations are initialized with a steady-state RANS calculation using the realizable k-ε turbulence model [39] with enhanced wall treatment (EWT) [40]. The unsteady calculations utilize 20 iterations per time step. The scaled residuals for all equations fall below 1×10^{-5}. Data sampling is started after 20 revolutions of the turbine and continue for another 10 revolutions in order to ensure that the change in C_P between 2 subsequent revolutions is below 0.2%, as discussed in more detail in section 3.1.

2.4. Reference case

A reference case detailed in Table 5 is defined for the sensitivity analyses in section 3.

Table 2
Test matrix for the sensitivity study of the domain size. All sizes are given in turbine diameters (D). Note that for clarity the reference case (shown with †) is listed four times (once for each parameter).

Parameter	d_i	d_o	W	BR (D/W)	d_c	Domain size (L × W)	# cells	dθ
Distance to inlet (d_i)	2.5	25	20	5%	1.5	27.5 × 20	384,238	0.1°
	5					30 × 20 †	395,851	
	7.5					32.5 × 20	406,219	
	10					35 × 20	411,219	
	12.5					37.5 × 20	416,144	
	15					40 × 20	421,219	
Distance to outlet (d_o)	5	6	20	5%	1.5	11 × 20	372,203	
		10				15 × 20	381,563	
		15				20 × 20	392,863	
		20				25 × 20	394,943	
		25				30 × 20 †	395,851	
		55				60 × 20	419,705	
Domain width (W)	5	25	10	10%	1.5	30 × 10	377,819	
			20	5%		30 × 20 †	395,851	
			40	2.5%		30 × 40	432,651	
			70	1.43%		30 × 70	487,483	
Diameter of rotating core (d_c)	5	25	20	5%	1.25	30 × 20	379,926	
					1.5	30 × 20 †	395,851	
					2	30 × 20	502,399	

Table 3
Test matrix for the study of dθ. All sizes are given in turbine diameters (D).

Parameter	dθ (°)	dt (s)	d_i	d_o	W	BR	d_c	Domain size (L × W)	# cells
Azimuthal increment (dθ)	0.05	1.41665×10^{-5}	5	25	20	5%	1.5	30 × 20	395,851
	0.1	2.08333×10^{-5}							
	0.5	1.41665×10^{-4}							
	1.0	2.08333×10^{-4}							
	2.0	5.6666×10^{-4}							
	5.0	1.41665×10^{-3}							
	10.0	2.08333×10^{-3}							

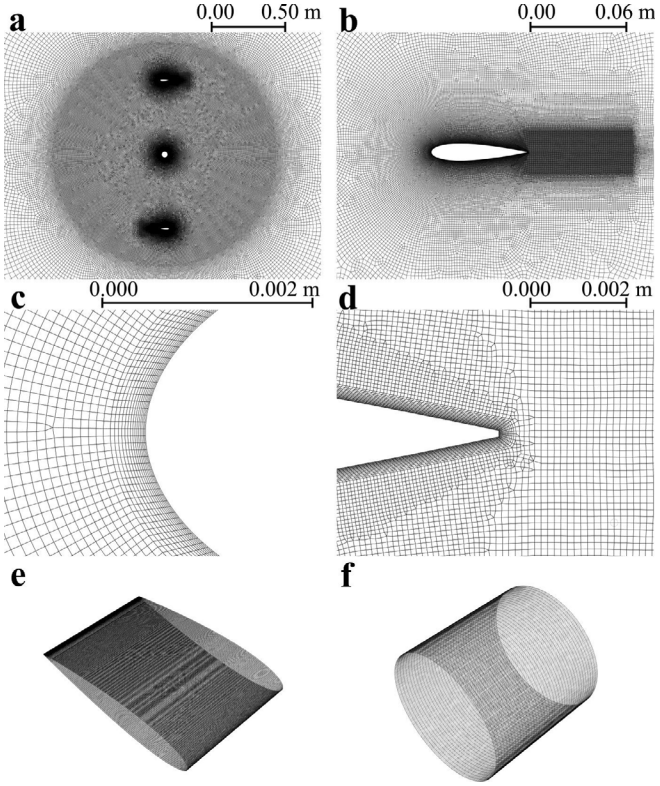

Fig. 2. Computational grid: (a) Near the rotating core; (b) Near the airfoil; (c) Airfoil leading edge; (d) Airfoil trailing edge; (e) 2.5D airfoil; (f) 2.5D shaft.

Table 4
Details of the computational grids.

	Grid size	Cells	Maximum y^+ on blades	Maximum y^+ on shaft
2D	Coarse	395,851	4.0	2.0
	Medium	755,782	2.8	1.5
	Fine	1,730,604	2.0	1.0
2.5D	Coarse	26,851,100	4.0	2.0

3. Revolution and grid convergence analysis

3.1. Revolution convergence analysis

In order to investigate the number of revolutions of the turbine required before a statistically steady flow field is obtained and data sampling can be started, the simulation for the reference case is performed for a total of 100 revolutions. Analysis of the time history of C_P (see Fig. 3) and C_T, calculated using Eqns. (4) and (5) over 1 revolution of the turbine, shows that after 20 revolutions the change in the two parameters between two successive revolutions of the turbine drops below 0.2% and 0.1%, respectively, and that the difference between the values at 20 (30) revolutions and at 100 revolutions is 2.41% (1.06%). Therefore the simulations are considered to have reached a statically steady state after 20–30 revolutions. This convergence criterion is stricter than the value found by Trivellato and Raciti Castelli [19] but in agreement with the findings from Balduzzi et al. and Lam and Peng [12,41].

Table 5
Details of the reference case.

Domain size	30D × 20D (Length × Width)
Grid size	Coarse (395,851 cells)
Azimuthal increment	0.1°
Turbulence model	4-equation Transition SST [37]
Revolutions	30

$$C_P = \frac{M\Omega}{qU_\infty A} \tag{4}$$

$$C_T = \frac{T}{qA} \tag{5}$$

3.2. Grid convergence analysis

In order to investigate the dependence of the results on the computational grid the simulation for the reference case is performed on three different grids: coarse, medium and fine (see Table 4). These grid sizes represent a systematic uniform doubling of the amount of cells between successive grid pairs. This allows the Grid Convergence Index (GCI) to be employed to quantify the discretization error [42]. The GCI is calculated based on C_P values using a safety factor (F_s) of 1.25. The GCI^{coarse} and GCI^{fine} for the coarse-medium grid pair are determined to be 6.1 × 10^{-3} (1.48%) and 3.5 × 10^{-3} (<1%) respectively. The reduction of the discretization error as a function of grid size is shown in Fig. 4, where the slope confirms that the solution is second order accurate. Furthermore, the instantaneous moment and power coefficients (C_m) of the turbine in the last revolution are compared for the three grids in order to further investigate the grid dependence of the results (see Fig. 5). It can clearly be seen that there is a negligible difference between the three curves taken in the wake of the shaft ($\theta = 270°$): the maximum absolute difference is 2.5 × 10^{-3} (which results in less than 1% difference in C_P). The difference which can be observed can be attributed to a slight improvement in the prediction of flow separation on the shaft which also has a very limited effect on the turbine C_P: values obtained for the coarse, medium and fine grids are 0.410, 0.412 and 0.413. Based on these results the coarse grid was selected for the rest of the calculations, also as the mid plane for the 2.5D grid.

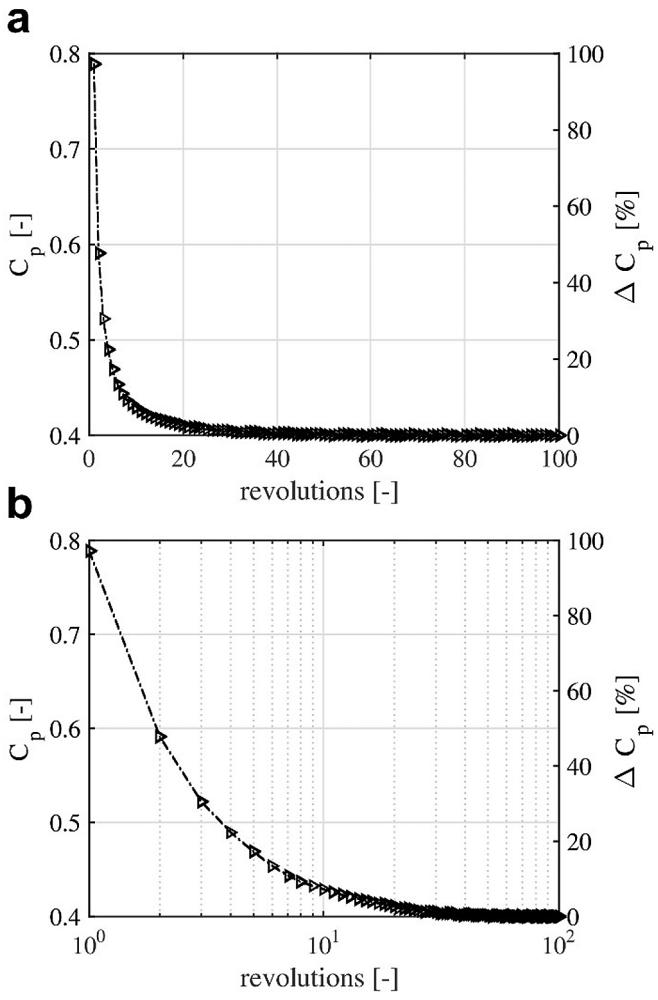

Fig. 3. History of power coefficient C_P and its relative change with respect to the last revolution ΔC_P of the turbine for 100 revolutions of the reference case in (a) normal and (b) log-scale.

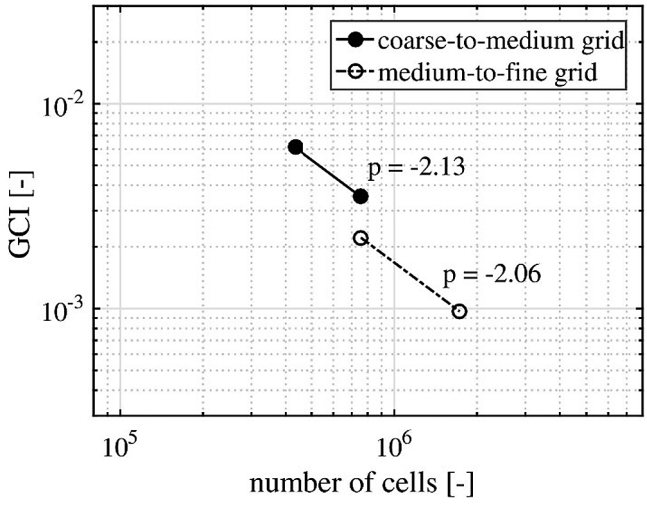

Fig. 4. Grid Convergence Index (GCI) for the three grids employed in this study; 'p' shows the slope of the line.

4. Validation study

The calculated C_P of the reference case (both for the 2D and 2.5D simulations) is approximately 0.41 which, when compared to the reported value of the experiment [9], 0.40, amounts to a deviation of 2.5%. The normalized averaged (over 10 turbine revolutions) streamwise and lateral velocities in the near wake of the turbine at different downstream locations (x/R = 2.0, 2.5, 3.0, 3.5 and 4.0: see Fig. 6) are compared with experimental data from Tescione et al. [9]: see Figs. 7–8. The values for the 2.5D simulation and the experiment correspond to the midplane of the turbine. The average deviation of the normalized values from the experimental data is shown in Table 6. It can be seen that overall there is good agreement both for the 2D and 2.5D results with experimental data for both streamwise and especially lateral velocities. The following observations can be made:

- Self-induction (decrease in the velocity magnitude as the wake develops further downstream) was predicted for the streamwise velocity, in agreement with experimental findings [9,43];

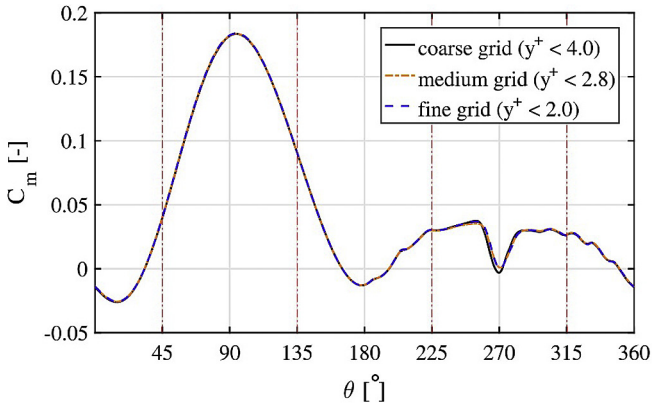

Fig. 5. Instantaneous moment coefficient for the last revolution versus azimuth for different grids. The y^+ values given in the legend correspond to the maximum values on the airfoils. The definition of azimuth θ is shown in Fig. 1: $\theta = 0°$ corresponds to the blade in the most windward location.

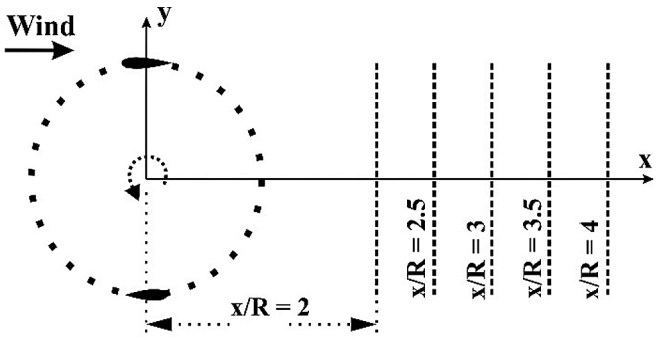

Fig. 6. Downstream measurement locations in the near wake.

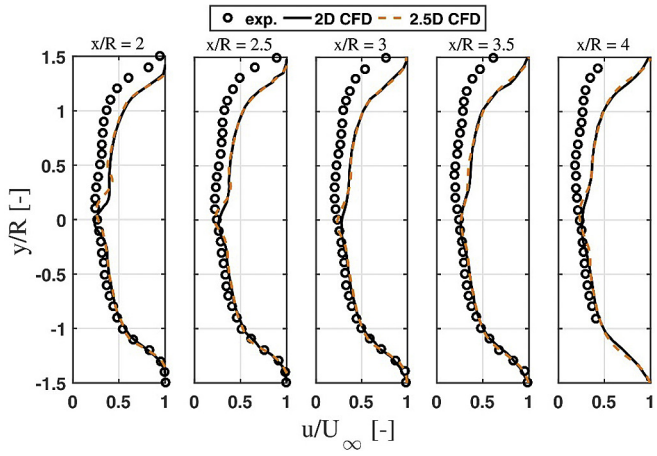

Fig. 7. Normalized averaged (over 10 turbine revolutions) streamwise velocity in the near wake of the turbine compared with experiment [9].

- The recovery of the velocity was not started at the most downstream location (x/R = 4) for the studied case which is in agreement with results of Tescione et al. [9];
- The decrease in the profile slopes for the lateral velocity is well predicted. This shows that the induction for the cross-stream velocity as well as the wake expansion rate is already decreasing at the studied downstream locations in the near wake [9];

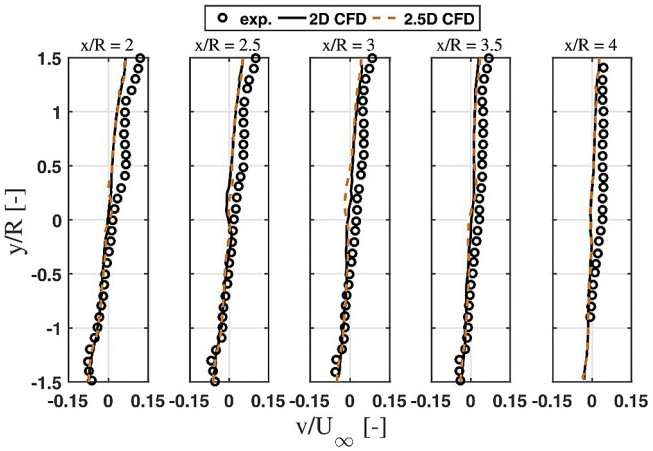

Fig. 8. Normalized averaged (over 10 turbine revolutions) lateral velocity in the near wake of the turbine compared with experiment [9].

- The experimentally observed drift of the position of zero cross-stream velocity toward the leeward side (y/R < 0) for further downstream locations is also present in the calculation results.

However, while the agreement with experiments for both streamwise and cross-stream velocities is generally good on the leeward side (y/R < 0), significant discrepancies occur on the windward side (y/R > 0). The experimentally observed asymmetry in the wake of the turbine is not predicted. This asymmetry was suggested [44] to be due to the fact that the blades on the windward side face lower experienced velocity as they move towards the wind while on the leeward side the opposite occurs. This can also be expressed in terms of forces on blades: the blades (at zero pitch angle) receive a net force in the negative y-direction and in reaction they exert a net force in the positive y-direction pushing the flow windward [45].

Several (mutually dependent) reasons for the observed discrepancy are listed below:

- The asymmetry has been thought [9] to be partly due to the rotation of the shaft (Magnus effect). As the pressure distribution over a cylinder changes with respect to the surface roughness [46–49], the wake deflection angle due to this effect will be influenced by the surface roughness. No value for surface roughness was reported in the experiment and the parameter was thus not considered in the simulation: this might be a reason for the observed discrepancy. Furthermore, based on the experimental observation [9], the shaft wake is deflected towards the windward side. Future work is needed to investigate the effect of the shaft surface roughness on the turbine wake asymmetry.
- The geometrical simplifications in the modeling are another possibility for this discrepancy where the airfoils' spokes and connecting struts to the turbine tower were neglected in order to facilitate high-quality grid generation. The simplifications result in ignoring the velocity deficit created in the wake of these less-aerodynamic bodies as well as the vortex shedding due to large separation on such elements.
- The larger deviation on the windward side is partly expected to be due to the lower resistance of flow to separation in this region compared to the leeward side, which poses more difficulties for prediction of the flow using URANS CFD [50,51]. The lower resistance on the windward side is due to the fact that in this region the blade moves against the freestream direction and

Table 6
Average deviation of the normalized averaged (over 10 turbine revolutions) streamwise and lateral velocity in the near wake from the experimental values [9].

x/R			2.0	2.5	3.0	3.5	4.0
Average deviation (%)	u/U_∞	2D	8.6	10.0	11.8	12.6	16.4
		2.5D	8.4	9.7	11.5	12.1	15.9
	v/U_∞	2D	2.5	2.3	2.2	2.3	2.9
		2.5D	2.3	2.2	2.5	2.3	2.9

therefore resembles the typical case of an upstream-moving wall. The boundary layer in this case is more prone to separation in comparison to the leeward side where the situation is similar to a downstream-moving wall [52]. Additionally, the higher tendency of the flow to separate on the windward side can also result in larger separation on the less aerodynamic bodies (connecting struts, which are not present in the CFD simulation) while moving through this region. Thus they will have a larger effect on the wake on the windward side (another possible reason for the wake asymmetry) which is ignored in the CFD calculation due to geometrical simplification.

- Lastly, the discrepancy might be due to the limitation of RANS modeling in the prediction of complex flow phenomena such as the wakes of bluff bodies [50,51] and blade-wake interactions [53]. This experimentally-observed asymmetry has not been predicted by previous CFD studies either [41,54,55] where the turbine was operating in the same range of tip speed ratios and larger deviation on the windward side is reported. Therefore, further research might be required in order to enable the CFD simulations to predict the VAWT's wake with higher accuracy.

Despite the observed discrepancy in the wake, one should note that:

- The difference between the calculated turbine power coefficient (C_P) and the value reported in the experimental work [9] is only 2.5%.
- The average deviation between the CFD results (both 2D and 2.5D) and experimental data for the normalized lateral velocity for different downstream locations is <3%.
- The average deviation between the CFD results (both 2D and 2.5D) and experimental data for the normalized streamwise velocity for different downstream locations is 8–16%.

Due to the negligible difference between the 2D and 2.5D results, the former was selected for the rest of the studies in view of grid and computational economy.

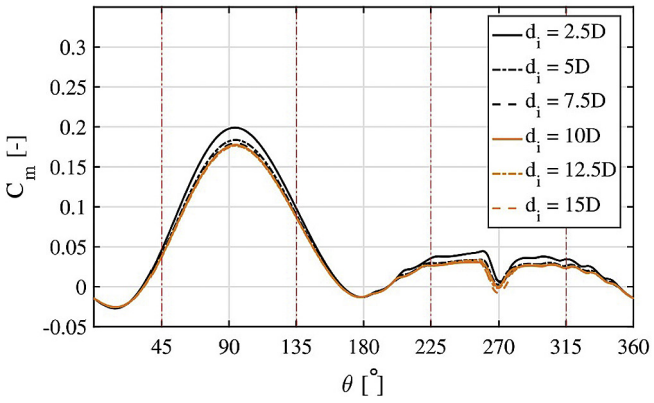

Fig. 9. Instantaneous moment coefficient for the last revolution versus azimuth for domains with different d_i.

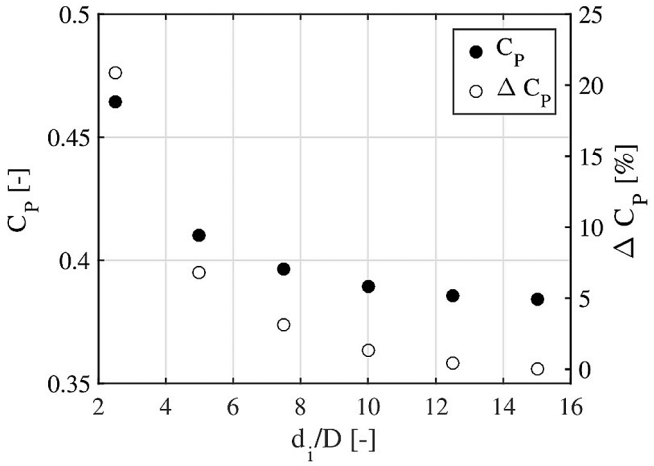

Fig. 10. Power coefficient for the last revolution as a function of d_i and its relative change with respect to the domain with largest d_i of 15 D.

5. Sensitivity analysis: effect of domain size

5.1. Distance to the inlet

The effect of the distance of the inlet of the domain to the turbine center on the moment coefficient (C_m) of the turbine (Fig. 9) is found to be significant as large differences are observed especially in the upwind and downwind quartiles. This difference is also observed in the C_P of the turbine (Fig. 10) where the value obtained for the domain with $d_i = 2.5D$ is more than 20% larger than that for the domain with $d_i = 15D$. A monotonic and asymptotic decrease of C_P with increasing d_i is found, where the difference between values for the domains with $d_i = 10D$ and 15D is approximately 1%. This difference is small enough that, in view of the larger discrepancies observed in the previous section, $d_i = 10D$ can be seen as a safe minimum value in order to avoid significant overestimation of the performance of the turbine.

In order to further study the effect of inlet distance, the normalized streamwise velocity profiles at different upstream locations of the turbine (Fig. 11) are compared. The presence of the induction field of the turbine at upstream locations as far as $d_{up} = 7.5D$ can clearly be observed (Fig. 12). Therefore, domains with smaller d_i result in an overestimation of streamwise velocity upstream of the turbine which results in higher incoming velocities at the turbine incident distance $d_{up} = 0.5D$ (see Fig. 13). As the power of the turbine is proportional to the third power of the incoming velocity the small overestimation of streamwise velocity results in a large overestimation of C_P of the turbine: e.g. 1.69% overestimation of incoming velocity magnitude at the turbine incident distance $d_{up} = 0.5D$ (averaged over y for $-0.5 < y/D < 0.5$) resulted in 5.46% overestimation of C_P for domain with d_i of 5D and 10D.

As shown in Fig. 12, the blockage due to the presence of the turbine in the domain results in acceleration of the flow in lateral

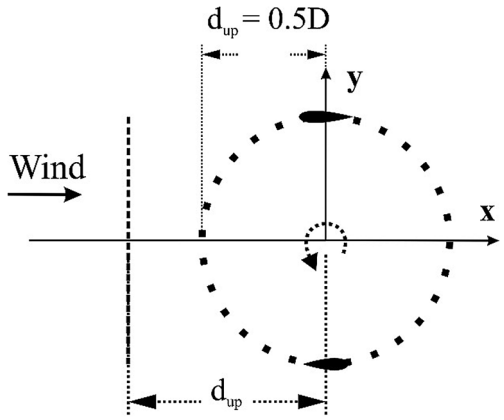

Fig. 11. Schematic showing the upstream distance from the domain inlet to the turbine center of rotation.

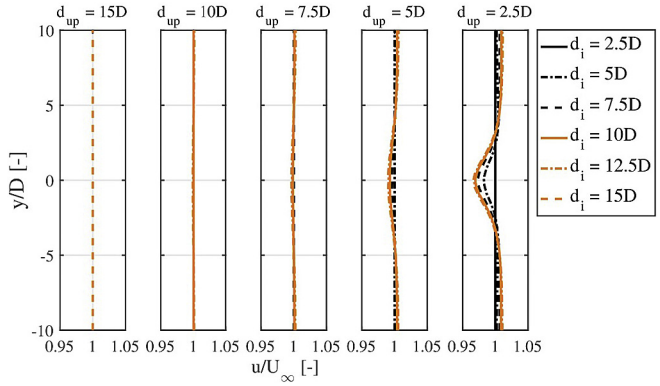

Fig. 12. Normalized averaged (over 10 turbine revolutions) streamwise velocity profiles at different upstream locations for domains with various d_i.

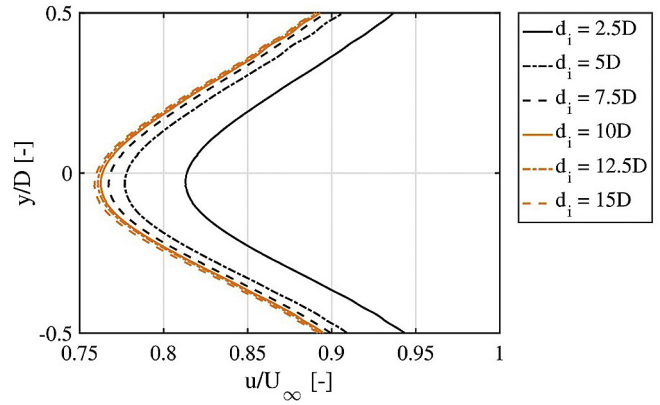

Fig. 13. Normalized averaged (over 10 turbine revolutions) streamwise velocity profiles at turbine upstream distance (d_{up} = 0.5D) for domains with various d_i.

locations (−3 > y/D and y/D > 3) when the flow approaches the turbine (d_{up} < 5D). This is consistent with the continuity equation when considering the large deceleration of the flow in the turbine stagnation region (−3 < y/D < 3). The effect of blockage of the turbine on the predicted power performance of the turbine (C_P) is found to be negligible for blockage ratio less than 5% as comprehensively discussed in section 5.3.

The turbine induces an asymmetry on the streamwise velocity profiles downstream of the turbine (see Fig. 7). The possible explanations for this asymmetry and the reasons why it is not well predicted by the CFD simulation are explained in section 4. Fig. 12 shows that the downstream asymmetry has negligible effect on the streamwise velocity profiles upstream of the turbine.

On the other hand, studies of urban flows [15,16,35,36] have revealed that turbulence intensity may decay as a function of distance in the domain. Such a decay is also observed here (Fig. 14). Therefore, one should distinguish between the inlet turbulence intensity and the incident turbulence intensity [35,56]. Both should be reported in both computational and experimental studies, and care must be taken that the turbulence intensity matches target values at the correct location.

5.2. Distance to the outlet

Fig. 15 shows the moment coefficient versus azimuth for the last revolution of the turbine for domains with various outlet distances d_o. Small differences can be observed in the C_P of the turbine (Fig. 16), especially for the domain with 10D distance to the outlet, although the effect is still less than 1%. The largest difference is observed for the domain with d_o = 6D where the deviation from C_P for the domain with d_o = 55D is approximately 2.35%.

In order to further investigate the reason for this difference the pressure coefficient at the outlet is compared for domains with different outlet distances d_o: see Fig. 17. Generally, either a constant or a surface-averaged gauge pressure can be specified at a pressure outlet, where for incompressible cases a value of zero is most commonly used. In the present study, setting a constant gauge

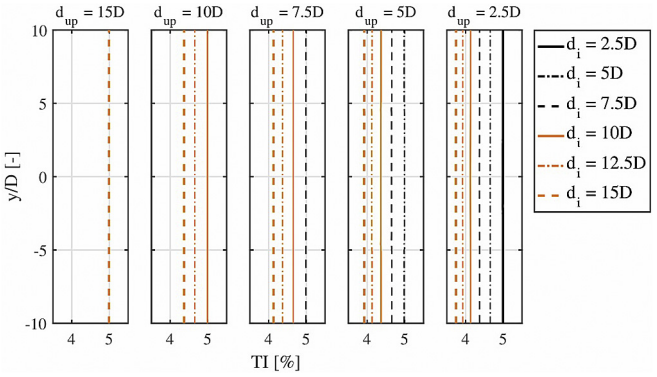

Fig. 14. Averaged (over 10 turbine revolutions) turbulence intensity (TI) at different upstream locations for domains with various d_i.

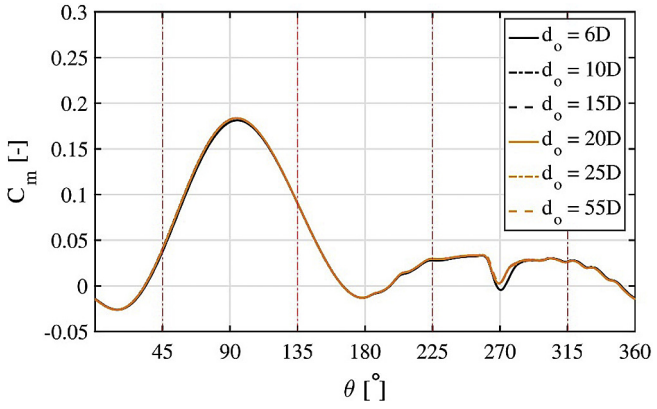

Fig. 15. Instantaneous moment coefficient for the last revolution versus azimuth for domains with different d_o.

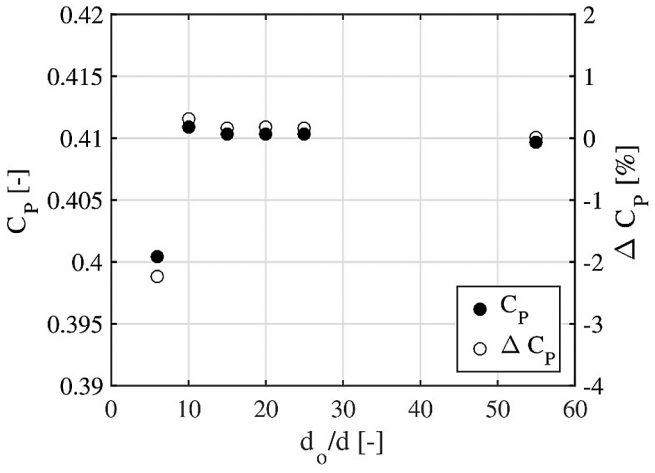

Fig. 16. Power coefficient for the last revolution as a function of d_o and its relative change with respect to the domain with largest d_o of 55 D.

pressure value is found to result in higher scaled residuals. The surface-averaged gauge pressure specification provides an effective solution to this problem and is therefore the method used in this study. For either method the outlet should be placed far enough from the turbine in order to prevent the flow from being artificially modified due to the proximity of the outlet.

Fig. 17 shows that a minimum distance of 25D to the outlet results in a uniform outlet pressure coefficient, with a negligible difference compared with the case with a d_o = 55D. This small difference (≈0.1%) is thought to be a result of the better wake recovery due to the longer distance to the outlet. However, apparently a non-zero value for gauge pressure at the outlet has no discernible effect on the performance of the turbine within the studied range. Therefore, for the given λ the minimum distance of 10D investigated here represents a safe choice. The difference in C_P between this case and a d_o of 55D is about 0.3%.

It should be noted that the minimum d_o might be related to the length of the wake of the turbine. The contour of non-dimensional velocity magnitude of the flow over the turbine and in the near wake shown in Fig. 18 implies that the length of the wake is approximately 12 times the diameter of the turbine at the given λ, calculated from the center of rotation of the turbine and defined at $U/U_\infty = 0.98$. For the present case the minimum required d_o at this λ was therefore roughly equal to the length of the wake of the turbine while the domain with smaller d_o resulted in a significant

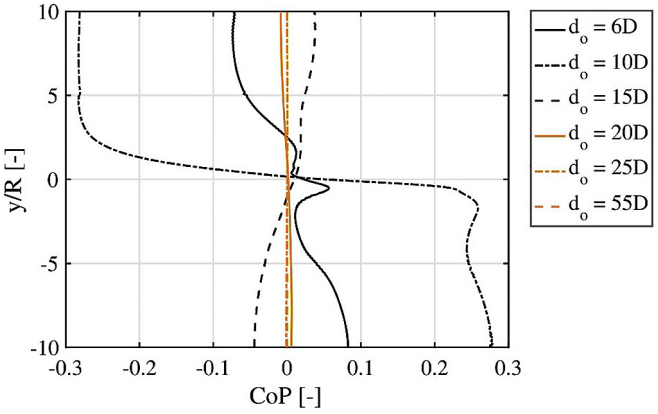

Fig. 17. Averaged (over 10 turbine revolutions) pressure coefficient CoP at the domain outlet for domains with different distances to the outlet.

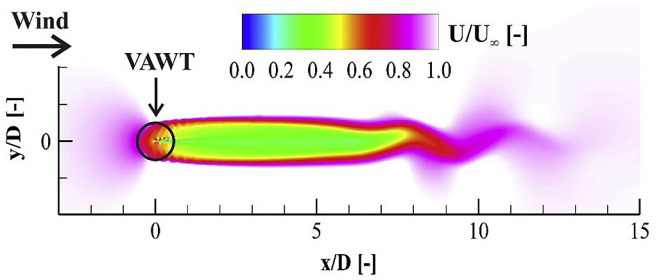

Fig. 18. Contour of normalized instantaneous velocity magnitude showing the wake of the turbine where the blades are positioned at the most windward and leeward locations: the black circle shows the rotor diameter.

difference. It can be inferred that the latter was most likely due to a cutting of the wake by the domain outlet and therefore incomplete development of the wake. However, it is important to note that currently no conclusion on the dependency of the d_o to the turbine wake length can be made and as the length of the wake of the turbine is dependent on λ, future research at other tip speed ratios is needed to investigate this.

5.3. Domain width (blockage ratio)

The blockage ratio for the 2D calculation of a VAWT is defined as the ratio of the turbine diameter (D) and the domain width (W), Eqn. (6):

$$BR = \frac{D}{W} \tag{6}$$

The effect of domain width on the moment coefficient of the turbine is given in Fig. 19. It is more pronounced than what was found for the outlet distance (cf. Fig. 15) but less than the effect of the inlet distance (cf. Fig. 9). The power coefficient C_P and its relative change with respect to the widest domain are shown in Fig. 20. Again a more significant effect on C_P was found than for the outlet distance, with a relative difference in C_P values between blockage ratios of 10% and 5% of approximately 3.85%. An overprediction of C_P is found for the larger blockage ratio due to artificial acceleration of the flow. A domain width of 20D (blockage ratio of 5%) was found to be sufficient as the difference in C_P when increasing the width to 70D (blockage ratio of 1.43%) was 0.2%. This was found to be of the same order as the value recommended in the best practice guidelines for CFD simulation of urban flows [14–16] (maximum blockage ratio of 3%) and aeronautical and vehicle aerodynamics

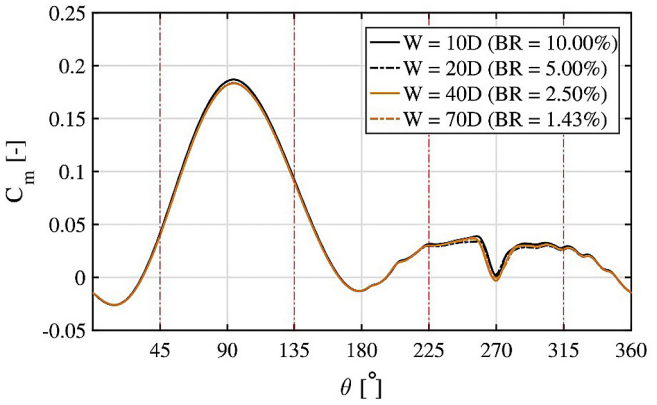

Fig. 19. Instantaneous moment coefficient for the last revolution versus azimuth for domains with different width.

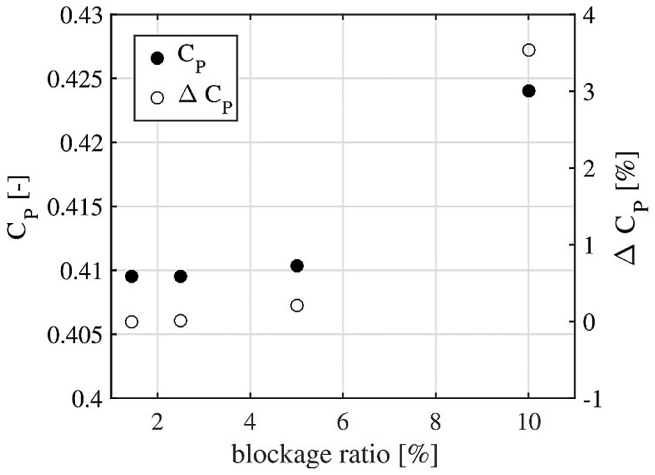

Fig. 20. Power coefficient for the last revolution as a function of blockage ratio and its relative change with respect to the widest domain.

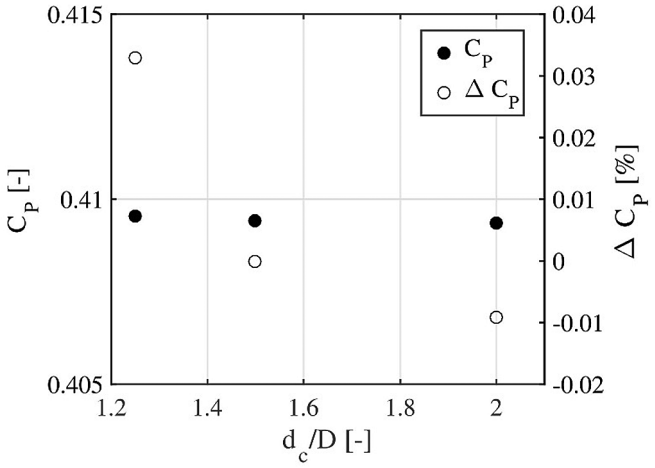

Fig. 22. Power coefficient for the last revolution as a function of diameter of d_c and its relative change with respect to d_c = 1.5D for domains with different d_c.

[57,58] (maximum blockage ratio of 5–7.5%).

5.4. Diameter of the rotating core

The moment coefficients for domains with three different diameters of the rotating core (1.25D, 1.5D and 2D) are shown in Fig. 21. It can be seen that the effect of the diameter of the rotating core on the performance of the turbine is negligible. The power coefficient C_P and its relative change for the three domains shown in Fig. 22 indicate that the difference is less than 0.4% between the domains with core diameters of 1.25D and 1.5D and less than 0.2% between the domains with core diameters of 1.5D and 2D. This is partly attributed to the fact that the change in d_c does not impact the blockage ratio and the distance between the side borders of the rotating core and the lateral boundaries does not have any notable effect. Based on the performance comparison and considering the increase in the number of cells with increasing diameter of the rotating core (while keeping the edge sizing on the periphery of the rotating core constant) (see Table 2) one can safely opt for the domain with a 1.25D core diameter. However, it is good to note that a larger distance between the airfoils and the domain interface between the rotating core and fixed domain can help with high-quality grid generation. It allows for a more gradual coarsening of the grid from sufficiently small cells near the airfoil towards larger cells at the interface and also helps to keep the grid fine in the wake of the blades if required (e.g. for smaller tip speed ratios where the flow is strongly separated). For these reasons the domain with a 1.5D core diameter is preferred in the present study, despite a 4% increase in the number of cells. On the other hand, the domain with a 2D core diameter resulted in 27% more cells (while keeping the edge sizing on the periphery of the rotating core constant) which was deemed unnecessary.

6. Sensitivity analysis: effect of azimuthal increment

A plot of C_m versus azimuth for various $d\theta$ is shown in Fig. 23. From these results it is clear that simulations with $d\theta$ values of 10.0° and 5.0° are largely unable to predict the moments on the blades. This is also confirmed by the time history of C_P shown in Fig. 24 and final C_p values in Fig. 25, where a large underprediction is found. $d\theta$ values of 2.0° and 1.0° also tend to underpredict C_P, however to a much smaller amount. Between $d\theta$ values of 0.5°, 0.1° and 0.05° a negligible difference in C_P is observed.

Based on this comparison $d\theta = 0.5°$ is found to be a safe choice at the given λ. However, it is important to note that this value is limited to moderate tip speed ratios where the flow is not strongly separated. Any change in the flow which might lead to a larger separation such as operating at lower λ, introducing pitch angles to the blades or application of thicker or asymmetric airfoils would require a smaller $d\theta$ in order to accurately predict the aerodynamics

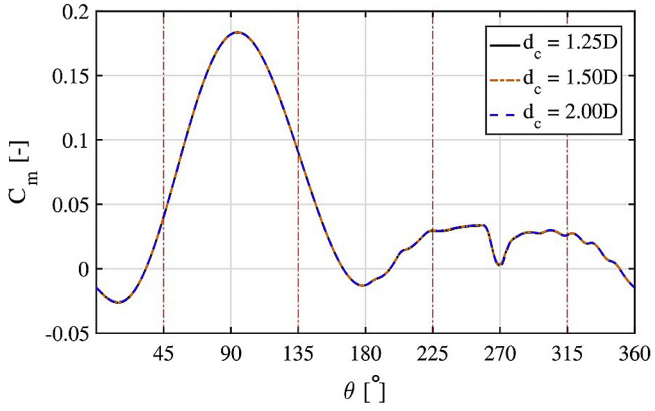

Fig. 21. Instantaneous moment coefficient for the last revolution versus azimuth for domains with different d_c.

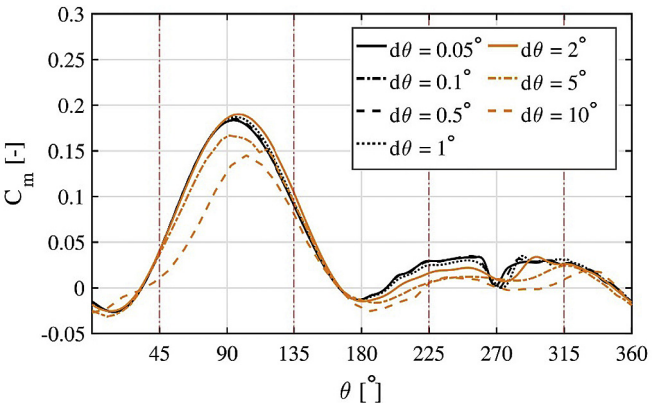

Fig. 23. Instantaneous moment coefficient for the last revolution versus azimuth for various azimuthal increments.

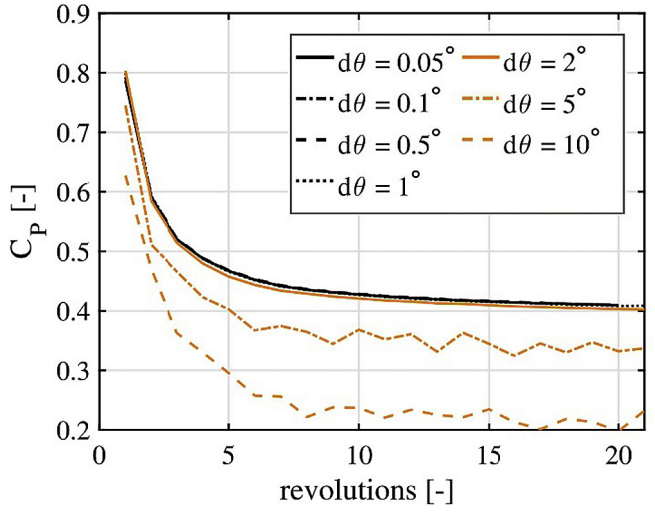

Fig. 24. History of power coefficient C_P for various azimuthal increments.

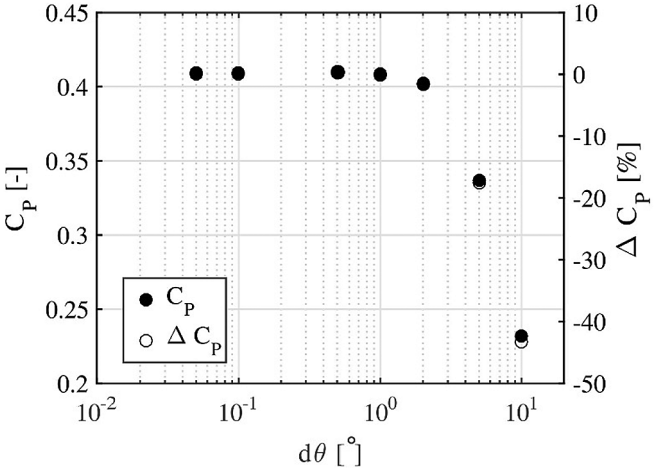

Fig. 25. Power coefficient for the last revolution for various azimuthal increments.

and performance of VAWTs.

7. Discussion

It is important to once again highlight the conditions where the aforementioned minimum requirement in sections 5 and 6 are recommended for. Most importantly, as explained in section 2.1 the selection of the symmetric airfoil and the moderate tip speed ratio is made in order to avoid the dynamic stall: this limits the complexities of the flow and the dynamic loads on blades. Therefore, the recommendations are made for cases where flow is not strongly separated on the blades and the blades do not experience dynamic stall. Therefore, the variations of angle of attack for the corresponding airfoil should always be carefully checked for the given operating conditions to characterize the regime of the flow before using the given recommendations. For such cases where the flow might be strongly separated; i.e. low tip speed ratios, asymmetric airfoils, introducing pitch angles to blades, etc.; finer azimuthal increment might be required. Moreover, the choice of low-solidity is made to limit the blade-wake interactions and flow curvature effects and for high-solidity VAWTs finer azimuthal increments might be required in order to more accurately predict the corresponding flow complexities. On the other hand, the calculations were based on assuming the midplane of a high aspect ratio VAWT where the 3D tip effects are very small. Therefore, for very low aspect ratio (<0.5 [9]) 3D tip effects can be significant and other requirements might be needed. Lastly, the simulations are based on a small-scale VAWT corresponding to the medium-range (chord-based) Reynold number 100,000–500,000, however, no significant difference in domain size and azimuthal increments are foreseen for CFD simulation of larger multi-MW VAWTs ($Re > 1 \times 10^6$) where the turbine is low-solidity, high aspect ratio operating at moderate to high tip speed ratios and the flow is not strongly separated on blades. On the other hand, lower chord-based Re ($< 1 \times 10^5$) might require finer azimuthal increment due to higher tendency of the flow to separation. One should also note that the minimum requirement for the azimuthal increment is given for a URANS calculation while for LES and hybrid RANS-LES calculations, the time step should be set in order to have Courant–Friedrichs–Lewy (CFL) number < 1 in the LES region of the domain so that the match between the spatial and temporal resolution ensures the filtered eddies are resolved properly.

Given the highlighted limitations to generalize the minimum requirements for the domain size and azimuthal increment, future work is required in order to investigate the dependence of these requirements on the tip speed ratio and solidity of the turbine. Additionally, confirmation of the identified minimum requirements for high Reynolds number ($Re > 1 \times 10^6$) might also be of interest for accurate CFD simulation of large multi-MW VAWTs.

8. Conclusions

The current study investigated the effect of the domain size (distance from the turbine center to the inlet and outlet, domain width), diameter of the rotating core and azimuthal increment on the performance of a low-solidity VAWT rotating at a moderate tip speed ratio of 4.5 and a medium range (chord-based) Reynolds number (100,000–200,000) using 2D URANS CFD simulations. Results of a 2.5D simulation showed negligible difference with 2D results for the studied case representing the midplane of a high aspect ratio turbine where the 3D tip effects are negligible. The results were validated with experimental data.

The following conclusions were obtained for the studied turbine:

1) The results sampled before 20 revolutions of the turbine will result in large overestimation of the performance of the turbine. The minimum number of revolutions in order to obtain a converged solution is 20–30 where the change in C_P between 20 (30) and 100 revolutions is 2.41% (1.06%).
2) The minimum distance from the turbine center to the inlet of $d_i = 10D$ is found to minimize the effect of the domain inlet on the performance of the turbine. Smaller distances result in overestimation of C_P of the turbine as a result of overestimation of the velocity magnitude at the turbine incident ($d_{up} = 0.5D$). However, a decay in the turbulence intensity is observed in the domain from the domain inlet to downstream. Therefore, one should distinguish between the inlet turbulence intensity and at the incident turbulence intensity. Both should be reported in both computational and experimental studies, and care must be taken that the turbulence intensity matches target values at the correct location.
3) A minimum distance from the turbine center to the outlet of $d_o = 10D$ is found to minimize the effect of the domain outlet on the performance of the turbine. This distance is found to be approximately equal to the wake length of the turbine. Smaller distances will result in underestimation of the C_P of the turbine which might be due to cutting the turbine wake where the wake

is not fully developed. Larger distances will not have any unwanted effect on the results as they also allow the full development of the wake.

4) A domain width of W = 20D is found to minimize the effect of the blockage on the results. This is equivalent to blockage ratio (D/W) of 5%.
5) A minimum diameter of the rotating core equal to $d_c = 1.5D$ was found to both minimize the effect of the size of the rotating core on the results as well ensure ease of meshing and minimum computational costs.
6) A minimum azimuthal increment of $d\theta = 0.5^\circ$ was found to minimize the effect of the temporal resolution on the performance of the turbine.

The conclusions above are limited to a low-solidity high-aspect ratio VAWT operating at a moderate tip speed ratio where the flow is not strongly separated. Large separation of the flow (and occurrence of dynamic stall) on the blades of the turbine due to the choice of the airfoil, the low tip speed ratio or the pitch angle on the blades might demand a larger domain size and a finer azimuthal increment. Furthermore, the high solidity will also increase the flow complexities and might demand finer azimuthal increment. Future work is needed to address the limitations of the current study and further generalize the identified minimum requirements for the azimuthal increment and domain size.

Acknowledgement

The authors would like to acknowledge support from the European Commission's Framework Program Horizon 2020, through the Marie Curie Innovative Training Network (ITN) AEOLUS4FUTURE - Efficient harvesting of the wind energy (H2020-MSCA-ITN-2014: Grant agreement no. 643167) and the TU1304 COST ACTION "WINERCOST". The authors gratefully acknowledge the partnership with ANSYS CFD. This work was sponsored by NWO Exacte Wetenschappen (Physical Sciences) for the use of supercomputer facilities, with financial support from the Nederlandse Organisatie voor Wetenschappelijk Onderzoek (MP-297-14) (Netherlands Organization for Scientific Research, NWO).

References

[1] U.S. Paulsen, H.A. Madsen, K.A. Kragh, P.H. Nielsen, I. Baran, J. Hattel, E. Ritchie, K. Leban, H. Svendsen, P.A. Berthelsen, DeepWind-from idea to 5 MW concept, Energy Procedia 53 (2014) 23–33.
[2] M.R. Islam, S. Mekhilef, R. Saidur, Progress and recent trends of wind energy technology, Renew. Sustain. Energy Rev. 21 (2013) 456–468.
[3] A. Tummala, R.K. Velamati, D.K. Sinha, V. Indraja, V.H. Krishna, A review on small scale wind turbines, Renew. Sustain. Energy Rev. 56 (2016) 1351–1371.
[4] S. Gsänger, J.D. Pitteloud, Small Wind World Report Summary, World Wind Energy Association (WWEA), 2015.
[5] B. Blocken, 50 years of computational wind engineering: past, present and future, J. Wind Eng. Ind. Aerodyn. 129 (2014) 69–102.
[6] A.J. Buchner, M.W. Lohry, L. Martinelli, J. Soria, A.J. Smits, Dynamic stall in vertical axis wind turbines: comparing experiments and computations, J. Wind Eng. Ind. Aerodyn. 146 (2015) 163–171.
[7] C. Simão Ferreira, G. van Kuik, G. van Bussel, F. Scarano, Visualization by PIV of dynamic stall on a vertical axis wind turbine, Exp. Fluids 46 (1) (2008) 97–108.
[8] A. Bianchini, F. Balduzzi, G. Ferrara, L. Ferrari, Virtual incidence effect on rotating airfoils in Darrieus wind turbines, Energy Convers. Manag. 111 (2016) 329–338.
[9] G. Tescione, D. Ragni, C. He, C. Simão Ferreira, G.J.W. van Bussel, Near wake flow analysis of a vertical axis wind turbine by stereoscopic particle image velocimetry, Renew. Energy 70 (2014) 47–61.
[10] C. Simão Ferreira, H.A. Madsen, M. Barone, B. Roscher, P. Deglaire, I. Arduin, Comparison of aerodynamic models for vertical axis wind turbines, J. Phys. Conf. Ser. 524 (012125) (2014).
[11] M. Islam, D. Ting, A. Fartaj, Aerodynamic models for Darrieus-type straight-bladed vertical axis wind turbines, Renew. Sustain. Energy Rev. 12 (4) (2008) 1087–1109.
[12] F. Balduzzi, A. Bianchini, R. Maleci, G. Ferrara, L. Ferrari, Critical issues in the CFD simulation of Darrieus wind turbines, Renew. Energy 85 (2016) 419–435.
[13] A. Rezaeiha, I.M. Kalkman, B. Blocken, Effect of Pitch Angle on Power Performance and Aerodynamics of a Vertical axis Wind Turbine, 2016 (under review).
[14] J. Franke, A. Hellsten, H. Schluzen, B. Carissimo, Best Practice Guideline for the CFD Simulation of Flows in the Urban Environment, COST, Hamburg, Germany, 2007.
[15] B. Blocken, Computational Fluid Dynamics for urban physics: importance, scales, possibilities, limitations and ten tips and tricks towards accurate and reliable simulations, Build. Environ. 91 (2015) 219–245.
[16] Y. Tominaga, A. Mochida, R. Yoshie, H. Kataoka, T. Nozu, M. Yoshikawa, T. Shirasawa, AIJ guidelines for practical applications of CFD to pedestrian wind environment around buildings, J. Wind Eng. Ind. Aerodyn. 96 (10–11) (2008) 1749–1761.
[17] C.-J. Bai, W.-C. Wang, Review of computational and experimental approaches to analysis of aerodynamic performance in horizontal-axis wind turbines (HAWTs), Renew. Sustain. Energy Rev. 63 (2016) 506–519.
[18] A. Bechmann, N.N. Sørensen, F. Zahle, CFD simulations of the MEXICO rotor, Wind Energy 14 (5) (2011) 677–689.
[19] F. Trivellato, M. Raciti Castelli, On the Courant–Friedrichs–Lewy criterion of rotating grids in 2D vertical-axis wind turbine analysis, Renew. Energy 62 (2014) 53–62.
[20] M. Elkhoury, T. Kiwata, E. Aoun, Experimental and numerical investigation of a three-dimensional vertical-axis wind turbine with variable-pitch, J. Wind Eng. Ind. Aerodyn. 139 (2015) 111–123.
[21] C. Simão Ferreira, H. Bijl, Gv Bussel, Gv Kuik, Simulating dynamic stall in a 2D VAWT: modeling strategy, verification and validation with particle image velocimetry data, J. Phys. Conf. Ser. 75 (012023) (2007).
[22] B. Shahizare, N. Nazri Bin Nik Ghazali, W. Chong, S. Tabatabaeikia, N. Izadyar, Investigation of the optimal omni-direction-guide-vane design for vertical axis wind turbines based on unsteady flow CFD simulation, Energies 9 (3) (2016) 146.
[23] N.N. Sørensen, J.A. Michelsen, S. Schreck, Navier-Stokes predictions of the NREL phase VI rotor in the NASA Ames 80 ft × 120 ft wind tunnel, Wind Energy 5 (2–3) (2002) 151–169.
[24] H. Sarlak, T. Nishino, L.A. Martínez-Tossas, C. Meneveau, J.N. Sørensen, Assessment of blockage effects on the wake characteristics and power of wind turbines, Renew. Energy 93 (2016) 340–352.
[25] I. Ross, A. Altman, Wind tunnel blockage corrections: review and application to Savonius vertical-axis wind turbines, J. Wind Eng. Ind. Aerodyn. 99 (5) (2011) 523–538.
[26] T.Y. Chen, L.R. Liou, Blockage corrections in wind tunnel tests of small horizontal-axis wind turbines, Exp. Therm. Fluid Sci. 35 (3) (2011) 565–569.
[27] A. Biswas, R. Gupta, K.K. Sharma, Experimental investigation of overlap and blockage effects on three-bucket Savonius rotors, Wind Eng. 31 (5) (2007) 363–368.
[28] C.M. Parker, M.C. Leftwich, The effect of tip speed ratio on a vertical axis wind turbine at high Reynolds numbers, Exp. Fluids 57 (5) (2016).
[29] Y. Kim, Z.-T. Xie, Modelling the effect of freestream turbulence on dynamic stall of wind turbine blades, Comput. Fluids 129 (2016) 53–66.
[30] P. Bachant, M. Wosnik, Effects of Reynolds number on the energy conversion and near-wake dynamics of a high solidity vertical-axis cross-flow turbine, Energies 9 (73) (2016).
[31] I. Paraschivoiu, Wind Turbine Design: with Emphasis on Darrieus Concept, Polytechnic International Press, Montréal, Québec, 2009.
[32] W.A. Timmer, Two-dimensional low-Reynolds number wind tunnel results for airfoil NACA 0018, Wind Eng. 32 (6) (2008) 525–537.
[33] C. Simão Ferreira, The Near Wake of the VAWT: 2D and 3D Views of the VAWT Aerodynamics, PhD, TU Delft, 2009.
[34] ANSYS, ANSYS® Fluent Theory Guide, Release 16.1, ANSYS, Inc., 2015.
[35] B. Blocken, J. Carmeliet, T. Stathopoulos, CFD evaluation of wind speed conditions in passages between parallel buildings—effect of wall-function roughness modifications for the atmospheric boundary layer flow, J. Wind Eng. Ind. Aerodyn. 95 (9–11) (2007) 941–962.
[36] B. Blocken, T. Stathopoulos, J. Carmeliet, CFD simulation of the atmospheric boundary layer: wall function problems, Atmos. Environ. 41 (2) (2007) 238–252.
[37] F.R. Menter, R.B. Langtry, S.R. Likki, Y.B. Suzen, P.G. Huang, S. Völker, A correlation-based transition model using local variables—part I: model formulation, J. Turbomach. 128 (3) (2006) 413–422.
[38] R.B. Langtry, F.R. Menter, S.R. Likki, Y.B. Suzen, P.G. Huang, S. Völker, A correlation-based transition model using local variables—part II: test cases and industrial applications, J. Turbomach. 128 (3) (2006) 423–434.
[39] T. Shih, W.W. Liou, A. Shabbir, Z. Yang, J. Zhu, A new k-epsilon eddy-viscosity model for high reynolds number turbulent flows - model development and validation, Comput. Fluids 24 (3) (1995) 227–238.
[40] M. Wolfshtein, The velocity and temperature distribution of one-dimensional flow with turbulence augmentation and pressure gradient, Int. J. Heat Mass Transf. 23 (1969) 301–318.
[41] H.F. Lam, H.Y. Peng, Study of wake characteristics of a vertical axis wind turbine by two- and three-dimensional computational fluid dynamics simulations, Renew. Energy 90 (2016) 386–398.
[42] P.J. Roache, Quantification of uncertainty in computational fluid dynamics, Annu. Rev. Fluid Mech. 29 (1997) 123–160.
[43] D.B. Araya, J.O. Dabiri, A comparison of wake measurements in motor-driven

and flow-driven turbine experiments, Exp. Fluids 56 (7) (2015).
[44] V. Rolin, F. Porté-Agel, Wind-tunnel study of the wake behind a vertical axis wind turbine in a boundary layer flow using stereoscopic particle image velocimetry, J. Phys. Conf. Ser. 625 (012012) (2015).
[45] C. Simão Ferreira, F. Scheurich, Demonstrating that power and instantaneous loads are decoupled in a vertical-axis wind turbine, Wind Energy 17 (3) (2014) 385–396.
[46] D. Lakehal, Computation of turbulent shear flows over rough-walled circular cylinders, J. Wind Eng. Ind. Aerodyn. 80 (1999) 47–68.
[47] E. Achenbach, Influence of surface roughness on the cross-flow around a circular cylinder, J. Fluid Mech. 48 (2) (1971) 321–335.
[48] E. Achenbach, E. Heinecke, On vortex shedding from smooth and rough cylinders in the range of Reynolds numbers 6 $x10^3$ to 5 x 10^6, J. Fluid Mech. 109 (1981) 239–251.
[49] A. Rezaeiha, I.M. Kalkman, B. Blocken, Effect of the Shaft on the Aerodynamic Performance of an Urban Vertical axis Wind Turbine: a Numerical Study, 2017 submitted for publication.
[50] W. Rodi, Comparison of LES and RANS calculations of the flow around bluff bodies, J. Wind Eng. Ind. Aerodyn. 69–71 (1997) 55–75.
[51] H. Lübcke, S. Schmidt, T. Rung, F. Thiele, Comparison of LES and RANS in bluff-body flow, J. Wind Eng. Ind. Aerodyn. 89 (2001) 1471–1485.
[52] M. Gad-el-Hak, D.M. Bushnell, Separation control: review, J. Fluids Eng. 113 (1) (1991) 5–30.
[53] S. Lardeau, M.A. Leschziner, Unsteady RANS modelling of wake–blade interaction: computational requirements and limitations, Comput. Fluids 34 (1) (2005) 3–21.
[54] A. Posa, C.M. Parker, M.C. Leftwich, E. Balaras, Wake structure of a single vertical axis wind turbine, Int. J. Heat Fluid Flow 61 (A) (2016) 75–84.
[55] S. Shamsoddin, F. Porté-Agel, Large Eddy Simulation of vertical axis wind turbine wakes, Energies 7 (2) (2014) 890–912.
[56] B. Blocken, T. Stathopoulos, J. Carmeliet, Wind environmental conditions in passages between two long narrow perpendicular buildings, J. Aerosp. Eng. 21 (4) (2008) 280–287.
[57] S. Perzon, On blockage effects in wind tunnels – a CFD study, in: SAE 2001 World Congress, Detroit, Michigan, 2001.
[58] J.B. Barlow, W.H. Rae, A. Pope, Low Speed Wind Tunnel Testing, third ed., John Wiley and Sons, Inc, 1999.